Efficient light-trapping with quasi-periodic uniaxial nanowrinkles for thin-film silicon solar cells

Sanjay K. Ram[a,*], Derese Desta[b], Rita Rizzoli[c], Bruno P. Falcão[b], Emil H. Eriksen[a], Michele Bellettato[c], Bjarke R. Jeppesen[a], Pia B. Jensen[a], Caterina Summonte[c], Rui N. Pereira[b,d], Arne Nylandsted Larsen[a], Peter Balling[a]

[a]Department of Physics and Astronomy – iNANO, Aarhus University, Gustav Wieds Vej 14, DK-8000 Aarhus C, Denmark

[b]Department of Physics and I3N, University of Aveiro, Campus Universitário de Santiago, 3810-193 Aveiro, Portugal

[c]Istituto per la Microelettronica e Microsistemi (IMM)-Consiglio Nazionale delle Ricerche, via Gobetti 101, 40129, Bologna, Italy

[d]Walter Schottky Institut and Physik-Department, Technische Universität München, Am Coulombwall 4, 85748 Garching, Germany

*Address correspondence to E-mail: sanjayk.ram@inano.au.dk; sanjayk.ram@gmail.com

Keywords: Silicon thin-film solar cells; Photovoltaic devices; Nanowrinkles; Light-management; Nanomolding; Finite element method modeling

Abstract

Self-organizing nanopatterns can enable economically competitive, industrially applicable light-harvesting platforms for thin-film solar cells. In this work, we present transparent solar cell substrates having quasi-periodic uniaxial nanowrinkle patterns with high optical haze values. The self-organized nanowrinkle template is created by controlled heat-shrinking of metal-deposited pre-stretched polystyrene sheets. A scalable UV-nanoimprinting method is used to transfer the nanopatterns to glass substrates on which single-junction hydrogenated amorphous silicon *p-i-n* solar cells are subsequently fabricated. The structural and optical analyses of the solar cell show that the nanowrinkle pattern is replicated throughout the solar cell structure leading to enhanced absorption of light. The efficient broadband light-trapping in the nanowrinkle solar cells results in very high 18.2 mA/cm^2 short-circuit current density and 9.5% energy-conversion efficiency, which respectively are 35.8% and 39.7% higher than the values obtained in flat-substrate solar cells. The cost- and time-efficient technique introduces a promising new approach to customizable light-management strategies in thin-film solar cells.

1. Introduction

Light-management, consisting of different approaches aimed at increasing the charge-carrier generation by a better utilization of the incident light, has become an integral part of solar cell optimization in the endeavor towards thin-film devices with higher efficiencies at lower costs [1,2,3,4,5]. An extensive variety of light-trapping nanopatterns and nanostructures using different fabrication techniques are reported, achieving varying degrees of success in enhancing efficiencies in thin-film solar cells [6,7,8]. Nevertheless, competitive solar cell performance in terms of absolute efficiencies achieved and viability of industrial integration are crucial for translating any innovative light-trapping strategy into industrial implementation [9,10,11,12,13,14,15,16,17].

Most of the periodic and precise nano- and microtextured light-manipulating templates are fabricated using time- and cost-intensive techniques which work against cost-reducing strategies and are often difficult to integrate into existing large-area photovoltaic manufacturing processes. Self-organizing surface patterns have recently gained attention as simple low-cost nanofabrication solutions for applications in mechanical, optical, electrical and biomedical fields [18,19,20]. The potential of such self-organizing surface deformations for creating light-trapping nanopatterns in silicon thin-film solar cells is yet to be explored. The possibility of realizing multi-scale features by converting 2D sheets to 3D nanostructures to enable broadband light manipulation holds great promise for practical and effective photon-harvesting in thin film solar cells [21].

In this work, we report on highly efficient amorphous silicon (a-Si:H) thin-film solar cells grown in *p-i-n* configuration on a novel self-organized quasi-periodic nanowrinkle patterned substrate

fabricated with an inexpensive and straightforward technique. Both experimental and theoretical tools are employed to study the optical and electrical performance of the a-Si:H solar cells on nanowrinkle substrates. A strong enhancement in the performance of the nanowrinkle solar cell is observed in comparison to a planar solar cell which includes a 39.7% enhancement of energy-conversion efficiency. Our investigations reveal multi-scale nanowrinkle features as effective light-confining structures with potential for commercially adaptable light-harvesting strategy.

2. Experimental and modeling details

2.1. Nanowrinkle master-template fabrication

The complete fabrication process of the nanowrinkle textured substrates and the a-Si:H solar cells on them is shown using schematic illustrations in Fig. 1. A pre-stretched Shrinky Dinks® polystyrene (PS) sheet was used to fabricate the nanowrinkle template. A 20 nm thick Au layer was deposited on a 10×25 cm^2 sized sheet using an e-beam evaporation method. The edges of the shorter sides of the Au coated PS sheet were constrained by clamps to a metal plate underneath and heated in an oven (130 °C for 5 mins). The uniaxial compressive stress arising from the stiffness mismatch between the rigid metal film and the softer thermoplastic during the shrinkage creates buckling in the metal-coated surface leading to formation of uniaxial nanometer-scale wrinkles (as depicted schematically in Fig. 1(b)). The periodicity and the amplitude of the wrinkles in the metal-coated surface of the plastic can be tuned by altering the thickness of the metal layer [18]. In this work, the results of the nanowrinkles obtained with a 20-nm-thick gold layer are presented. The central part of the shrunken PS sheet with parallel nanowrinkles was cut out to be used as the master template. Subsequently, the gold layer from the nanowrinkles was etched out in aqua-regia solution, followed by cleaning and functionalization of the master

template with Trichloro (1H,1H,2H,2H-perfluorooctyl) silane (from Sigma Aldrich) using a vapor-phase technique to create an anti-sticking layer on its surface [14,22]. The anti-sticking layer allows a clean separation of the subsequent soft mold from the master template as well as reuse of the master template multiple times.

2.2. Soft-mold fabrication and UV-nanoimprinting

In the next step, the nanowrinkle pattern was transferred to a soft mold negative replica, and thence to a UV-lacquer-coated glass substrate using a UV-nanoimprinting technique, as shown in Fig. 1(e-g). Polydimethylsiloxane (PDMS) from Sylgard184, Dow Corning, was used to make soft and flexible molds. PDMS was prepared by mixing the base and the curing agent in a ratio of 10:1, degassed in vacuum, and poured on the template followed by curing at 50 ºC for 4 h in an oven. Anti-sticking coating was applied to the PDMS molds immediately after peeling them off the master templates. To replicate the nanowrinkle features on glass substrates, a UV curable lacquer, OrmoComp® (Micro Resist Technology GmbH), was used. The pre-cleaned glass (BOROFLOAT® 33) substrate was first coated with an adhesion promoter (OrmoPrime®) prior to spin coating the UV-lacquer. A PDMS mold having the negative impression of the nanowrinkle features was placed onto the UV-lacquer layer and a low pressure (5 psi) was applied during the nanoimprinting process in a Nanonex nanoimprinter (NX-2600) and UV light was irradiated for 1 minute for curing the polymer at room temperature.

2.3. Solar cell fabrication

To fabricate a-Si:H solar cells in superstrate configuration on the nanowrinkle substrates, a thin (30 nm thickness) dielectric layer (SiO_2) was first coated on the UV-cured lacquer to protect the solar cell from any diffusing organic impurities from the underlying polymer layer and to

provide a better adhesion for the subsequent transparent conducting oxide (TCO) layer. In the next step, the front TCO electrodes were deposited by rf-magnetron sputtering (rf-MS) technique at 200 °C in this sequence: first a 220 nm thick indium tungsten oxide (IWO) layer, and subsequently an aluminum doped ZnO (AZO) layer to protect the IWO layer from the reducing atmosphere of the H_2 plasma present during the solar cell fabrication. For IWO layer deposition, an In_2O_3 ceramic target containing 1 wt.% WO_3 was used [23]. The deposition was performed at 40 W rf power and 2.25 mTorr pressure of a mixture of Ar and O_2 gases, where 0.75% O_2 is diluted in Ar. The AZO layer was deposited using a ZnO ceramic target containing 2 wt% Al_2O_3 at 100 W rf power and 2.25 mTorr Ar pressure.

Single-junction, *p-i-n* type a-Si:H solar cells with ~300 nm thick absorber layer were grown on TCO-coated nanowrinkle substrates using a cluster-type radio frequency plasma-enhanced-chemical-vapor-deposition (RF-PECVD) reactor, at 13.56 MHz in the temperature range 120 °C to 170 °C using specific gas mixtures for each layer, in order to obtain the desired optical and electrical properties, in the following sequence: (1) an 18 nm *p*-type a-Si:C:H window layer using SiH_4, H_2, B_2H_6 and CH_4 gases, (2) a 6 nm thin undoped a-Si:C:H graded buffer layer using a SiH_4, CH_4 and H_2 mixture, (3) a 300 nm a-Si:H *i*-layer using a mixture of SiH_4 and H_2 in a ratio (= SiH_4/H_2) of 0.4. This ratio was found to be optimum for obtaining a conformal growth over the nanowrinkles. (4) Finally, a 35 nm thick *n*-type a-Si:H layer using a SiH_4, H_2 and PH_3 mixture. Hydrogen plasma treatment was performed at the interfaces. For comparison, reference solar cells were also fabricated under similar deposition conditions on a flat glass substrate using the same front electrode configuration as in the nanowrinkle substrate, and on a commercially available Asahi ANS10ME substrate (glass substrate coated with SnO_2:F as TCO) [24]. The back electrical contacts to the devices comprise of 30-nm-thick indium tin oxide (ITO) sputtered using

an In_2O_3 ceramic target containing 10 wt% SnO_2 at 150 °C, 40 W rf power and 14 mTorr Ar pressure, followed by a thermally-evaporated 200-nm-thick Ag layer. A metal shadow mask having 3 mm diameter holes was used to achieve the desired electrode dimensions. The three different types of solar cells are designated in this article by referring to their substrates; thus, the solar cells on the nanowrinkle substrate are designated as NW-SC, on the flat glass as Flat-SC and on the Asahi substrate as Asahi-SC.

2.4. Characterization studies

The surface topography of the substrates was studied using atomic force microscopy (AFM, Bruker Dimension Edge) and the cross-sectional analysis of the solar cell devices was carried out using a focused ion beam (FIB) instrument (FEI VERSA 3D) with a scanning electron microscope (SEM) attachment. The optical properties of the solar cell devices were studied using an optical spectrometer equipped with a 150 mm integrating sphere (Perkin Elmer Lambda 1050). The solar cell current density vs. voltage (*J*-*V*) characteristics were measured under one sun illumination (100 mW/cm^2 AM1.5 irradiance) using a calibrated Oriel solar simulator with a xenon arc lamp. For the angle-dependent short-circuit current density (J_{sc}) measurements, the *J*–*V* curves for different angles of the incident light were measured by rotating the sample-holder stage from 0° to 50° in steps of 10° (angle of incidence = angle of rotation). The tilt angle was determined with a protractor attached to the turnable sample holder. The arrangement is shown schematically in Fig. S1 (Supporting Information). To obtain light of different wavelengths, bandpass filters for 450 nm, 550 nm, 650 nm and 750 nm were placed between the sample and the sun simulator at a fixed position, perpendicular to the light beam. The sample holder was kept in a box lined with black paper on the inside to avoid any stray light falling on the sample during the measurements, with only an opening of 2×2 cm^2 at the top surface where the bandpass

filter (5×5 cm^2) was placed. The external quantum efficiency (EQE) measurements were performed using a setup calibrated with a reference cell, including a stable white lamp, a bias light, interference filters, a chopper and a lock-in amplifier. The chopped monochromatic light impinges on the whole device area and additional bias light was used to obtain the same cell J_{sc} as measured under the solar simulator. This is to ensure that the current signal at each wavelength is measured by means of the lock-in amplifier at approximately the real J_{sc} condition.

2.5. Modeling

The COMSOL Multiphysics simulation platform was employed for finite element method (FEM) modeling of the optical properties of the solar cells [25]. To construct a realistic model of the solar cell structure, AFM topographical data of the nanowrinkle substrate was used to construct a surface template. The structure was built as consecutive conformal layers. The layer thicknesses were estimated from the experimental growth rates of the individual layers and with the help of the cross-sectional FIB-SEM images of the fabricated devices (Fig. 1 (i)). To decrease the computational complexity, simulations were carried out in 2D slices (perpendicular to the nanowrinkles) of 10 μm width defining the x-axis. The (semi) infinite structure was emulated by mirroring the 10 μm slice in the y-axis and applying periodic boundary conditions on the sides. The top and bottom of the structure was truncated by perfectly-matched layers (PMLs). The structure was excited by a monochromatic plane wave propagating in the positive y-direction using a port boundary condition. To obtain the broadband spectrum, separate simulations were carried out in steps of 2 nm from 300–900 nm. The resulting data were smoothed using a Gaussian kernel corresponding to a coherence length of 20 μm in order to filter out diffraction effects induced by the periodic boundary conditions [26,27]. The final absorption data is averaged for the values obtained for parallel and orthogonal polarization. The refractive

indices of all layers except the Ag were obtained from spectroscopic ellipsometry, reflection, and transmission measurements. The optical data for Ag was taken from literature [28].

3. Results and discussion

Fig. 1(c) shows a photograph of the nanowrinkle PS template. The central part of the PS sheet, used for mold fabrication, is marked with a dashed line. The SEM image of this central part of the nanowrinkle template is shown in Fig. 1(d), where quasi-periodic uniaxial nanowrinkles are seen to fill up a large area without any visible cracks or structural defects. Although the nanowrinkles bifurcate and coalesce at places along the length of the pattern, they remain parallel and extend along the complete length of the scanned area [29]. A SEM image of the nanowrinkle features imprinted onto the glass substrate is shown in Fig. 1(h). The replication of the features from the PS template to the UV-lacquer has reasonably good fidelity, although the sharp and well-defined linear patterns of the template are seen to become somewhat smooth-edged on the UV-lacquer because of the transfer process using a soft PDMS mold. However, even with the same PDMS mold being used multiple times (we tried up to 10 repeated applications) to create the nanowrinkle patterns on the UV-curable lacquer, we found no difference in the surface features, as studied with AFM and SEM (results not shown here). We further tried imprinting with negative molds fabricated from hard PDMS, but a hard mold leads to formation of air pockets in the imprinted pattern, and breaking of the narrow ridges on removal. The SEM image of the Asahi TCO-glass substrate is shown in Fig. S2 in the Supporting Information. The surface of the Asahi TCO-glass substrate is randomly textured, with 200 – 500 nm wide irregular polygonal features, which are the top surfaces of the SnO_2:F crystalline grains.

The SEM images in Fig. 1(i) and (j) show FIB milled cross-sections of the solar cells deposited on the nanowrinkle substrate and on Asahi substrate, respectively. We see in the SEM image in Fig. 1(i) that the cross-sectional view of the nanowrinkles shows a series of unequal arches with some features as small as having 200 nm base-widths and some larger wrinkle arches spanning ~ 500 nm. The PDMS bridges some of the very narrow and deep furrows or folds between ridges that are formed in the template, so that such inter-ridge furrows in the nanowrinkle template are not replicated in the imprinted pattern. Instead, in the imprinted structure on the substrate, two adjoining ridges meet in a sharp linear groove leading to the arches seen in the cross-section, and at some points of coalescing channels, cusps are formed. Period doubling, commonly seen in wrinkling processes, is visible at places in the cross-sectional view. Some nanowrinkles are taller (~ 240 nm height from base to tip), flanked by shorter ones (50–70 nm). Overall, the cross-section of the nanowrinkles evinces a multi-scale features pattern [29]. It is also evident that the nanowrinkle pattern, characterized by quasi-periodic waves, is retained throughout the solar cell growth in each layer, resulting in a nanotextured ITO/Ag back-reflector.

We prevented the flattening out of the top layers of the solar cell by optimizing the deposition conditions for the absorber layer with the aim to balance conformal growth with good quality silicon layers [13]. A low hydrogen dilution in silane was used to maintain a conformal growth of the absorber layer, and interface-matching buffer layers and hydrogen-plasma treatments at the interfaces were judiciously used to ensure good optoelectronic properties of the solar cell on the textured substrates. With the progressive film growth, the replicated NW features, however, will have decreased sharpness of the features. In the context of the *p-i-n* NW-SC, the light coming in through the substrate falls on the features formed by the inversion of the substrate

features, so the wrinkles, grooves and cusp-like dents at the interfaces can be considered as valleys, ridges and bumps, respectively, for the incoming photons.

In order to assess the optical-scattering behavior of the nanowrinkle surfaces, total transmittance (T_T) and diffused transmittance (T_D) were measured on the uncoated (bare) and TCO-coated nanowrinkle substrates as a function of wavelength. The calculated spectral transmission haze factor H (= T_D/T_T) of these nanowrinkle substrates, denoting the capacity for random scattering of light to off-normal angles, are shown in Fig. 2(a). For comparison, the haze factor of a commercial Asahi substrate is also included in the graph. The particular Asahi substrate used in this study, Asahi ANS10ME, has better optical and electrical properties than the Asahi U TCO-glass substrate commonly used in research studies [24]. The haze values of the bare nanowrinkle substrate are similar to those of the Asahi substrate, although the contrast between the refractive indices of the nanowrinkle material (n ~1.5) and air (n = 1) is smaller than that between the Asahi substrate (refractive index, n ~2) and air. Once coated with the IWO (n ~ 2), the haze values of the TCO coated nanowrinkle surface are significantly higher than that of the Asahi substrate over the entire spectrum.

The total optical absorption (= 1 – total reflectance) spectra of the complete *p-i-n* solar cells (with Ag back-reflector) fabricated on nanowrinkle, Asahi and flat substrates, expressed as percentages, are shown in Fig. 2(b). The absorption spectrum of the Flat-SC exhibits peaks and valleys at various wavelengths, resulting from the interference created by the Fabry-Perot reflection of light at the planar interfaces between the layers with different refractive indices in the solar cell. In the textured solar cells, the interfaces between the different layers have nano-scale features that lead to diffuse reflection and randomized internal light paths, and thus to a diminishing of the interference phenomena. The optical absorption of the Asahi-SC is

predictably higher than that of the Flat-SC due to the surface textures optimally designed for broadband light-scattering [24]. A similar broadband enhancement in the optical absorption is also observed in the NW-SC, with more than 90% absorption over a broad spectral range from 400–650 nm, and more than 70% and 50% absorption at λ = 700 nm and λ = 800 nm, respectively.

The short wavelength light (< 500 nm) is absorbed mainly in the top layers of the solar cell, and does not reach the back reflector. In such a situation, the high absorption observed in the NW-SC compared to the Flat-SC (Fig. 2(b)) can be attributed completely to the improved in-coupling of light effectuated by the rough Si/TCO interfaces (TCO coated nanowrinkles), facilitated by the gradient of refractive indices of the consecutive layers of glass/UV-lacquer/TCO/a-Si:H (n = 1.5/1.5/2/4.5) [30,31]. Small features are known to play an important role in the in-coupling of light at short wavelengths [32]. Such features on the light-facing surface can be the ridges formed by the grooves and small bumps formed by the cusp-like dents between the nanowrinkles. At longer wavelengths (> 600 nm), where the light is poorly absorbed by the a-Si:H layer in a single pass, the absorption falls off abruptly beyond the bandgap edge in the Flat-SC, as seen in Fig. 2(b). The striking difference between the absorption curves of the Flat-SC and the textured solar cells in this part of the spectrum accentuates the effect of light-trapping inside the solar cell arising from the nanofeatures. The nanotextured silver back-reflector in the textured solar cells leads to multiple internal reflections of light over a broad range of angles with elongation of the optical path and a consequent enhancement of absorption, as observed for the NW-SC and Asahi-SC in the long wavelength region [32]. In addition, there may also be a contribution from confinement of light in the absorber layer, consistent with the coupling of light

into in-plane-guided modes, as typically seen with grating periods and wrinkles at this scale [19,33].

An optical modeling study of the solar cells (Flat-SC and NW-SC) was carried out to identify the absorption regions in the solar cells. Fig. 2(c) compares the FEM simulated total optical absorption spectra (average values of parallel and orthogonal polarization) of the *p-i-n* a-Si:H solar cells deposited on the flat and on the nanowrinkle substrates for an *i*-layer thickness of 300 nm. An agreement between the simulated and experimental absorption spectra of the Flat-SC validates the model and the selection of material optical parameters. Good qualitative resemblance is observed between the simulated and the experimentally obtained optical absorption profiles of the NW-SC. The cross-sectional profiles of the simulated absorption distribution in the NW-SCs, shown in Fig. 2(d-g), and in the Flat-SCs, shown in Fig. 2(h-k), are calculated for incident light of wavelengths 475 nm, 575 nm, 675 nm and 775 nm. Overall, the absorption is lower in the Flat-SC compared to the NW-SC, and progressively decreases for higher wavelengths. At the short wavelength (λ = 475 nm) the light is completely absorbed within the top 50-60 nm of the a-Si:H layer in both the NW-SC and the Flat-SC, as seen in Fig. 2(d) and (h), respectively. In Fig. 2(d), localized areas of enhanced absorption can be seen in the NW-SC at the concavities that may be grooves or cusp-like dents, while a uniform absorption is seen in the Flat-SC. At wavelengths ≥ 575 nm, the absorption distribution profiles of the Flat-SC device show alternating bands of high and low optical absorption due to Fabry-Perot resonances within the film. The increased absorption localized at the concavities is more prominently visible in the absorption distribution profile of NW-SC at 575 nm, Fig. 2(e). At longer wavelengths, the patterns of optical absorption in the NW-SC reveal distribution of trapped light within the absorber layer of the solar cell, Fig. 2 (e-g). At 675 nm and 775 nm, the absorption profiles of the

NW-SC display clear indication of light-trapping with high-absorption hot-spots (5 times higher than the average absorption) distributed throughout the a-Si:H absorber layer, which can contribute to effective photocarrier generation.

While the simulation study corroborates the experimental observation of the nanowrinkle features as a source of increased light-trapping, the amount of simulated absorption in the NW-SC is lower than the experimental results. Besides non-idealities in the simulation parameters, an important factor is the non-uniformity of the nanowrinkles in the z-direction. In the simulations carried out in 2D (xy-plane), the nanowrinkles are implicitly assumed to be perfectly homogeneous along the z-direction, while in reality the bifurcating and coalescing networks of nanoscale grooves between the wrinkles extend in the z-direction. Other than the grooves, the cusp-like dents are also potential sources of the absorption hot-spots, as seen in Fig. 2(d-g), but the total amount of neither can be approximated in the model calculations leading to slight underestimation of the absorption.

The *J-V* characteristics of the *p-i-n* solar cells fabricated on the flat, the Asahi and the nanowrinkle substrates are shown in Fig. 3(a). The deduced solar cell parameters are listed in Table 1. The energy-conversion efficiency (η) of the NW-SC is 9.5%, a boost of 39.7% over the 6.8% efficiency in the Flat-SC. The device fabricated on the Asahi substrate shows a high η = 10.1%, which is close to the reported efficiency records in single-junction a-Si:H solar cells (also on Asahi substrates) [6], indicating the effectiveness of the growth conditions selected for achieving conformal growth over textured surfaces. However, when it comes to the ability to generate a photocurrent, the NW-SC with its J_{sc} of 18.2 mA/cm^2 exhibits an outstanding 35.8% enhancement over the Flat-SC (J_{sc} = 13.4 mA/cm^2) and even outperforms the Asahi-SC (J_{sc} = 17.7 mA/cm^2), demonstrating the light-trapping efficacy of the nanowrinkles. The short-circuit

current in the NW-SC, to the best of our knowledge, is higher than the reported records of J_{sc} (before light soaking) in single-junction a-Si:H solar cells [6,34,35].

The lower fill factor (*FF*) of the Flat-SC compared to the NW-SC can originate from the higher series resistance in the Flat-SC device. This could be due to the differences between the thicknesses of the protective AZO layers (more electrically resistive than the IWO front electrode underneath) grown over the flat and the wrinkle surface. For a fixed short growth time aimed to achieve ~ 8 nm layer thickness over a flat surface, the actual resultant thickness of the layer over the textured surface will be lower. Similarly, the buffer layer found optimal for the NW-SC may turn out to be thicker (and not optimal) for the Flat-SC, when deposited for the same duration. The optimization of *p*/*i* and *n*/*i* interfaces using buffer layers has a significant effect on the open-circuit voltage (V_{oc}) and *FF*, but it does not drastically affect the short-circuit current. Thus, the solar cell architecture, which was optimized for the nanowrinkle substrates, is shown to be effective in maintaining a good balance between the V_{oc} and the *FF* in the NW-SC. The value of the $FF \times V_{oc}$ for the NW-SC is only slightly higher (3.3%) than that of the Flat-SC. Therefore the 39.7% higher efficiency of the NW-SC is completely attributable to the 35.8% improvement in the short-circuit current. The highest and lowest values of the device parameters (J_{sc}, V_{oc}, η and *FF*) achieved in each of the three types of solar cells can be seen in the graphical plots in Fig. S3 in the Supporting Information.

The wavelength-dependent EQE measured on the NW-SC, the Asahi-SC and the Flat-SC are shown in Fig. 3(b). In the NW-SC, a significant enhancement of the EQE in comparison to Flat-SC is observed over the whole spectral region. These EQE enhancements are consistent with the observed absorption enhancement shown in Fig. 2(b) for the solar cells grown on nanowrinkle surfaces. Furthermore, at smaller wavelengths, 400 nm < λ < 500 nm, the device made on the

nanowrinkle surface shows higher EQE than even the Asahi-SC, although the total optical absorption in the Asahi-SC and the NW-SC are similar in this part of the spectrum. Thus, the higher EQE in the NW-SC must stem from a lower parasitic absorption in the front electrode of the NW-SC compared to the Asahi-SC, and/or from better charge separation and collection in the NW-SC architecture. At longer wavelengths, the EQE values of the NW-SC are similar to those of Asahi-SC except in the vicinity of 650 nm where the performance of the Asahi-SC is higher.

There is a significant diurnal and seasonal variation in the angle and spectral composition of incident sunlight, which leads to variability in solar cell performance in field conditions. Therefore, the angular dependence of the photocurrent in the solar cell is relevant to predicting outdoor performance and to assess design efficacy. Apart from the change in the optical path in the solar cell with changing angles, the optical absorption behavior of the material also varies with the incidence angle, manifesting as a blue-shift of the interference maxima. The shift of the interference maxima to smaller wavelengths with increasing angle of incidence obeys the Bragg equation: $n\lambda_p = 2d \sin(\theta_i)$, where λ_p is the wavelength of the interference pattern and θ_i is the angle between the surface plane and the incident beam, d and n are the layer thickness and its refractive index respectively.

We studied and compared the effects of varying angles of different wavelengths of incident light on the optoelectronic properties of the three different solar cells. The angular dependence of J_{sc} of the Flat-SC, the Asahi-SC and the NW-SC for different wavelengths is shown as contour plots in Fig. 4(a), (b) and (c), respectively. The data plots of the angular dependence of J_{sc} are provided in Fig. S4 in the Supporting Information. In Fig. 4, the 0° angle of incidence in the y-axis of the graphs corresponds to the normally impinging light on the solar cell surface. To ensure a fair comparison between the J_{sc} values obtained for various solar cells at different

angles of incident light with varying wavelengths, the J_{sc} values were normalized by the maximum value of the J_{sc} obtained. In this case, the maximum J_{sc} was for the NW-SC at normal incidence with 550 nm light. The same experiment was repeated after rotating the NW-SC by 90° in the solar cell surface plane to rule out polarization effects; however, no difference between the J_{sc} values was observed. For a superstrate configuration solar cell, where light travels from air into glass, another consideration is the reflection of a fraction of the light at the glass surface itself, as described by Fresnel's equations. This fraction is low and constant up to a certain angle, Brewster's angle, above which the reflected fraction rises rapidly. Our measurements of angular dependence of electrical properties of the solar cells were carried out up to an angle of incidence of 50°, thus avoiding any significant reflections at the glass surface, since Brewster's angle for visible light (unpolarized) passing from air to glass is approximately 56°.

The color contour patterns of the normalized J_{sc} of the textured solar cells are impressively different from that of the Flat-SC. The position of the maximum photocurrent generation at normal incidence of light is at around 550-650 nm in all the solar cells, where light absorption takes place throughout the thickness of the a-Si:H layer. The visual contrast between the images arises from the intense red-orange glow in NW-SC contour map spreading wider and higher than the other two images. This signifies higher photocurrent generation in the NW-SC for a wider range of incident angles over a broad spectral range compared to the other two solar cells. In the Flat-SC, the increasing angle of the impinging light leads to a longer and oblique path of the photons in the solar cell, resulting in a high probability of substantial parasitic absorption of light by the front TCO and the *p*-layer. This is one of the reasons that results in a marked fall in the J_{sc} of the Flat-SC when the incidence angle of light increases, indicated in Fig. 4(a) by the appearance of the blue strip from 30° onwards at the 450 nm wavelength. This loss is mitigated

in the textured solar cells due to in-coupling of light at the textured TCO interfaces leading photons to reach the absorber layer. The detrimental effect of the absence of a light-trapping arrangement on the short-circuit current is also evident from the rapid fall of the normalized J_{sc} in the Flat-SC (Fig. 4(a)) at wavelengths beyond 710 nm (onset of the blue color, norm. J_{sc} < 20%), resembling its optical absorption spectrum in Fig. 2(b).

Light manipulation with self-organizing patterns like nanowrinkles is an emerging field. The photon harvesting potential of the nanowrinkles in thin film silicon solar cells is established in this work, but further studies are needed for a deeper exploration of the interrelationships of structural and optical properties of the nanowrinkles. There is still room for improvement in the *FF* and V_{oc} of the solar cell, which along with the application of an anti-reflection strategy can lead to even superior performance, possibly leading to efficiencies higher than current Si thin film solar cell records. The universality of the presented approach to light harvesting makes it applicable to thin-film solar cells based on any material in superstrate and substrate configurations, as well as to solar cells on unconventional substrates. The tunability of the nanowrinkle structure makes it particularly attractive for realizing patterns with sizes chosen to suit the bandgap properties of different absorber materials. Our method also allows the flexibility of using different kinds of TCOs including experimental high performance TCOs which can provide an alternative to the existing TCO-glass substrates. The simple technique is compatible with both large-area batch processing and roll-to-roll processing, without any significant impact on the existing manufacturing processes.

4. Conclusions

Quasi-periodic uniaxial nanowrinkles were created by controlled heating-induced shrinkage of gold deposited, pre-stretched polymer sheets and transferred to solar cell substrates using UV-nanoimprinting. Optical studies revealed excellent light-scattering haze factors in the nanowrinkle substrates and high broadband optical absorption in the single-junction a-Si:H *p-i-n* solar cells on these substrates. The effective light-trapping in the nanowrinkle solar cell is evinced by an enhancement of the photocurrent by 35.8% compared to flat-substrate solar cells, and the achievement of an unprecedented short-circuit current density of 18.18 mA/cm^2 in a single-junction a-Si:H solar cell. Model simulations were used to identify the regions of enhanced absorption of light, which were found to be concentrated in the grooves and cusps between the wrinkle walls. A high energy-conversion efficiency of 9.5% is obtained in the nanowrinkle solar cell which is 39.7% higher than the flat-substrate solar cell. The photocurrent generation in the solar cells on the nanowrinkle substrates is sustained better over a wide range of incident angles of light for a broad range of wavelengths than in the solar cells on flat and Asahi substrates. The inexpensive, versatile and effective technique of creating light-trapping nanowrinkles can be easily integrated with existing industrial manufacturing technologies of thin-film solar cells.

Author Contributions: The manuscript was written through contributions of all authors. All authors have given approval to the final version of the manuscript.

Conflict of Interest: The authors declare no competing financial interest.

Acknowledgment

The authors acknowledge support from the Danish Strategic Research Council under the project "Thin-film solar cell based on nanocrystalline silicon and structured backside reflectors (THINC)" as well as from the Innovation Fund Denmark under the project 'SunTune'. We thank Harish Lakhotiya for the optical measurements of the solar cells and Søren P. Madsen for his support for the computational analysis. D.D., B.P.F., and R.N.P. also acknowledge the financial support of the FCT (Fundação para a Ciência e a Tecnologia, Portugal) via projects PTDC/FIS/112885/2009, PTDC/CTM-ENE/2514/2012 and partially the project I3N (UID/CTM/50025/2013), financed by FCT/MEC and co-financed by FEDER under the PT2020 Partnership Agreement.

Appendix A. Supporting information

Supplementary data associated with this article can be found in the online version or from the author. It contains: (1) a schematic illustration of the arrangement for the measurement of angle dependent short-circuit current density of the solar cells; (2) a scanning electron microscopy image of the surface of the Asahi TCO-glass substrate; (3) a graphical plot of the experimentally obtained lowest and highest values of the device parameters (short-circuit current density, efficiency, open-circuit voltage and fill factor) of the flat, the Asahi and the nanowrinkle solar cells along with the parameter values of the devices reported in this article; and (4) a graph presenting the data of the short-circuit current densities of the flat, the Asahi and the nanowrinkle solar cells obtained at different incident angles and wavelengths of light.

List of Figures and Table:

Fig. 1(a) Schematic of a pre-stretched thermoplastic sheet coated with 20 nm Au. (b) Schematic illustration of the uniaxial nanowrinkles formed when the Au-coated sheet is heated with clamps at two opposite ends. (c) A photograph of the thermoplastic sheet after heat-shrinking, with dashed lines marking the central area used as a template for the mold fabrication. (d) A SEM image of the nanowrinkle template. (e) Schematic of fabrication of the PDMS mold from the template. (f) UV-nanoimprinting of the nanowrinkle pattern on the UV-lacquer-coated glass substrate with the PDMS mold. (g) Schematic view of the imprinted nanowrinkle substrate. (h) SEM image of the final nanowrinkle substrate. (i) and (j) SEM images of the FIB-milled cross-section of the *p-i-n* a-Si:H solar cells deposited on the nanowrinkle and the Asahi substrates, respectively. The top and the bottom electrode layers of the solar cells are falsely colored for better visualization and identification of the device structure.

Fig. 2(a) Wavelength dependence of the optical scattering measured as haze factor $(T_D/T_T)\%$ for the Asahi TCO-glass substrate (ANS10ME), bare (uncoated) and TCO-coated nanowrinkle substrates. (b) Total optical absorption spectra of the three solar cells: Flat-SC, Asahi-SC and NW-SC. (c) FEM simulated total optical absorption spectra of the Flat-SC and the NW-SC. (d) – (g) Calculated optical absorption distribution profiles of NW-SC at wavelengths 475 nm, 575 nm, 675 nm and 775 nm. For comparison, the distributions for the Flat-SC are shown in the smaller panels in the right column (h-k). The top dotted white lines demarcate the a-Si:H thin-film from the ITO of the back-reflector, while the middle lines indicate the interface between a-Si:H and front TCO electrode, and the bottom lines correspond to the TCO/substrate interface. The structure was excited by a monochromatic plane wave with an electric field amplitude of 1 V/m propagating in the positive y-direction using a port boundary condition.

Fig. 3(a) Current density vs. voltage (J–V) and (b) EQE characteristics of the solar cells deposited on flat, Asahi and nanowrinkle substrates.

Fig. 4 Color contour patterns of the normalized J_{sc} as functions of angle of incidences (ordinate) and wavelength (abscissa) obtained for the three solar cells deposited on (a) flat, (b) Asahi, and (c) nanowrinkle substrates. The J_{sc} values were normalized to the maximum value of the J_{sc}, which was obtained in the NW-SC at normal incidence of 550 nm light. Data were interpolated from measurements from 0° to 50°, in steps of 10°, for wavelengths of 450 nm, 550 nm, 650 nm and 750 nm.

Table 1. Summary of performance characteristics for the *p-i-n* a-Si:H solar cells fabricated on flat, Asahi, and nanowrinkle surfaces. The enhancements in J_{sc} and η are calculated using $\Delta J_{sc} = [(J_{sc\text{-textured-SC}} - J_{sc\text{-Flat-SC}})/ J_{sc\text{-Flat-SC}}]\times 100\%$ and $\Delta\eta = [(\eta_{\text{textured-SC}} - \eta_{\text{Flat-SC}})/ \eta_{\text{Flat-SC}}]\times 100\%$ respectively.

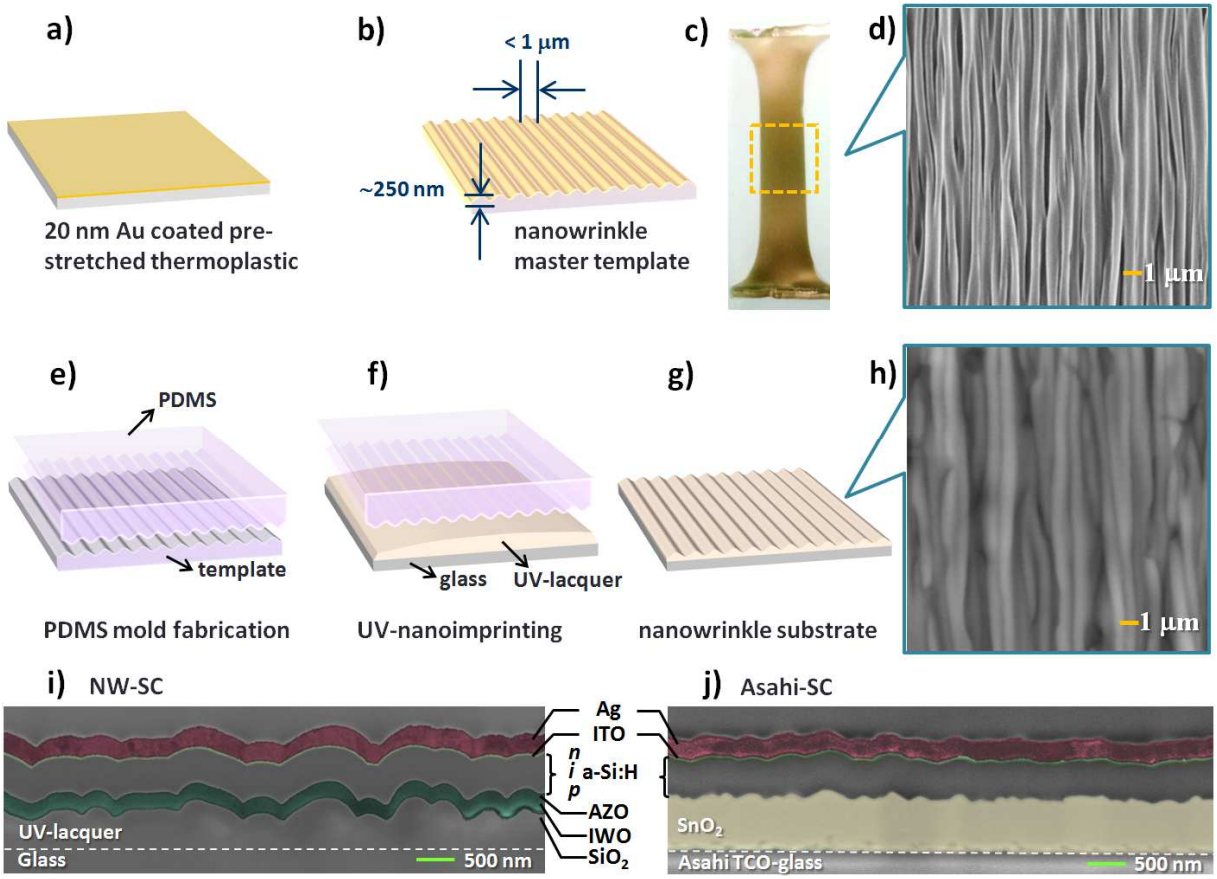

Fig. 1(a) Schematic of a pre-stretched thermoplastic sheet coated with 20 nm Au. (b) Schematic illustration of the uniaxial nanowrinkles formed when the Au-coated sheet is heated with clamps at two opposite ends. (c) A photograph of the thermoplastic sheet after heat-shrinking, with dashed lines marking the central area used as a template for the mold fabrication. (d) A SEM image of the nanowrinkle template. (e) Schematic of fabrication of the PDMS mold from the template. (f) UV-nanoimprinting of the nanowrinkle pattern on the UV-lacquer-coated glass substrate with the PDMS mold. (g) Schematic view of the imprinted nanowrinkle substrate. (h) SEM image of the final nanowrinkle substrate. (i) and (j) SEM images of the FIB-milled cross-

section of the *p-i-n* a-Si:H solar cells deposited on the nanowrinkle and the Asahi substrates, respectively. The top and the bottom electrode layers of the solar cells are falsely colored for better visualization and identification of the device structure.

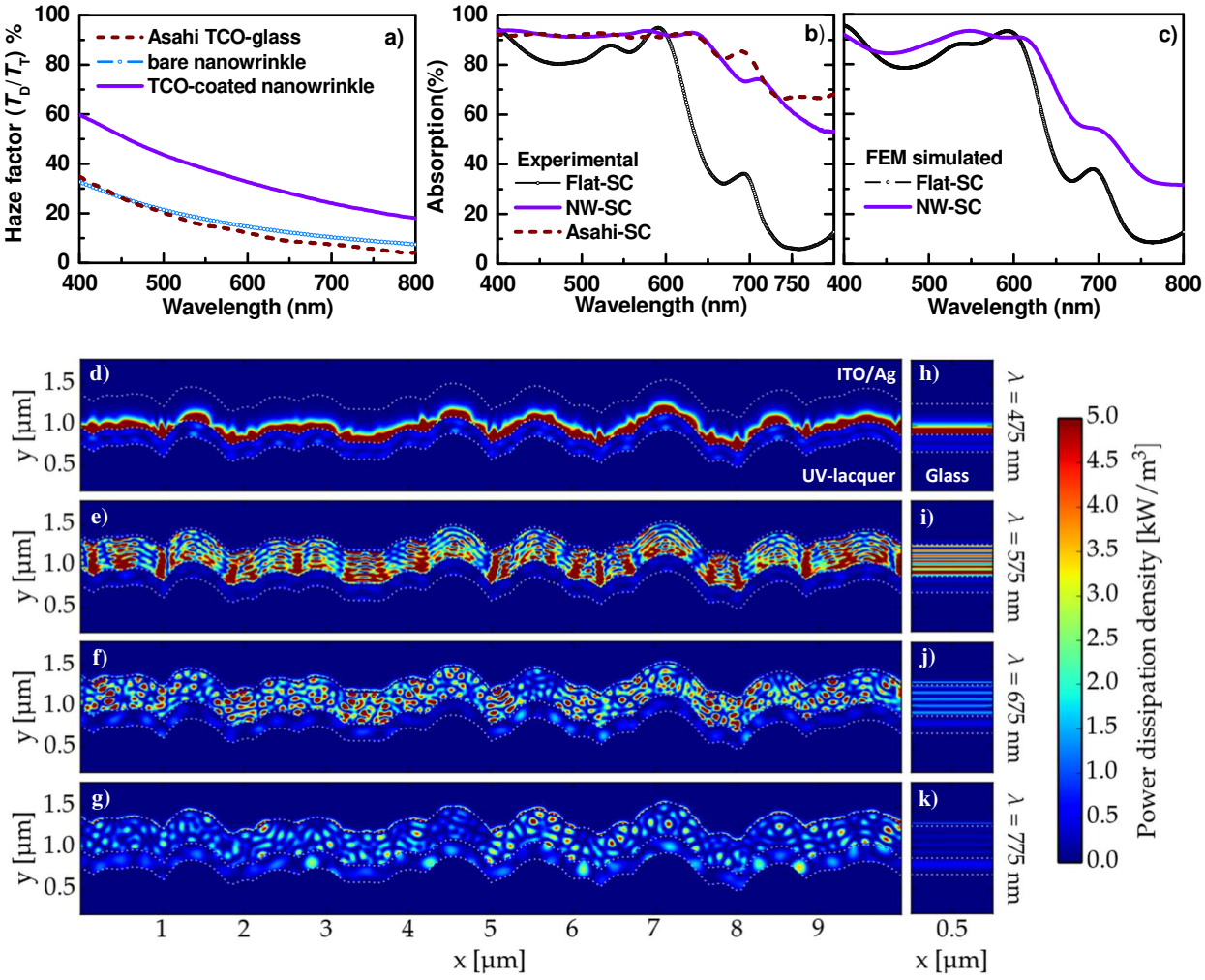

Fig. 2 (a) Wavelength dependence of the optical scattering measured as haze factor (T_D/T_T)% for the Asahi TCO-glass substrate (ANS10ME), bare (uncoated) and TCO-coated nanowrinkle substrates. (b) Total optical absorption spectra of the three solar cells: Flat-SC, Asahi-SC and NW-SC. (c) FEM simulated total optical absorption spectra of the Flat-SC and the NW-SC. (d) – (g) Calculated optical absorption distribution profiles of NW-SC at wavelengths 475 nm, 575 nm, 675 nm and 775 nm. For comparison, the distributions for the Flat-SC are shown in the smaller panels in the right column (h-k). The top dotted white lines demarcate the a-Si:H thin-

film from the ITO of the back-reflector, while the middle lines indicate the interface between a-Si:H and front TCO electrode, and the bottom lines correspond to the TCO/substrate interface. The structure was excited by a monochromatic plane wave with an electric field amplitude of 1 V/m propagating in the positive y-direction using a port boundary condition.

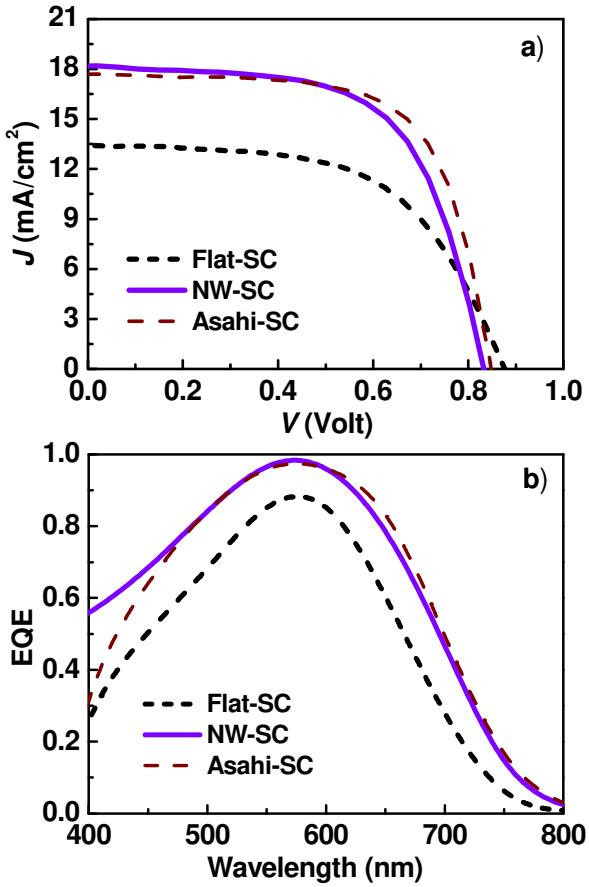

Fig. 3(a) Current density vs. voltage (*J*–*V*) and (b) EQE characteristics of the solar cells deposited on flat, Asahi and nanowrinkle substrates.

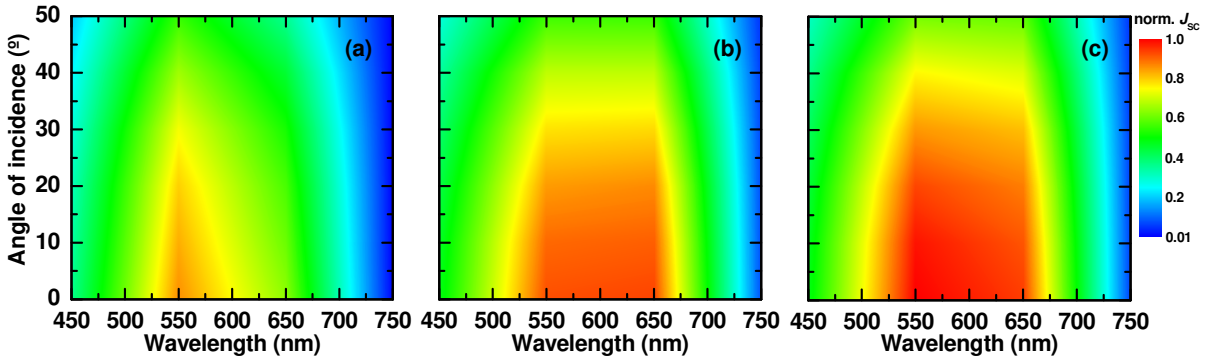

Fig. 4 Color contour patterns of the normalized J_{sc} as functions of angle of incidences (ordinate) and wavelength (abscissa) obtained for the three solar cells deposited on (a) flat, (b) Asahi, and (c) nanowrinkle substrates. The J_{sc} values were normalized to the maximum value of the J_{sc}, which was obtained in the NW-SC at normal incidence of 550 nm light. Data were interpolated from measurements from 0° to 50°, in steps of 10°, for wavelengths of 450 nm, 550 nm, 650 nm and 750 nm.

Table 1 Summary of performance characteristics for the *p-i-n* a-Si:H solar cells fabricated on flat, Asahi, and nanowrinkle surfaces. The enhancements in J_{sc} and η are calculated using $\Delta J_{sc} = [(J_{sc\text{-textured-SC}} - J_{sc\text{-Flat-SC}})/J_{sc\text{-Flat-SC}}]\times 100\%$ and $\Delta\eta = [(\eta_{textured\text{-SC}} - \eta_{Flat\text{-SC}})/\eta_{Flat\text{-SC}}]\times 100\%$, respectively.

Device	V_{oc} (mV)	FF (%)	η (%)	$\Delta\eta$ (%)	J_{sc} (mA/cm^2)	ΔJ_{sc} (%)
Flat-SC	876	58	6.8	--	13.4	--
NW-SC	833	63	9.5	39.7	18.2	35.8
Asahi-SC	849	67	10.1	48.5	17.7	32.1

References

[1] V. E. Ferry, M. A. Verschuuren, H. B. T. Li, E. Verhagen, R. J. Walters, R. E. I. Schropp, H. A. Atwater, A. Polman, Opt. Express 18 (2010) A237.

[2] H. W. Deckman, C. R. Wronski, H. Witzke, E. Yablonovitch, Appl. Phys. Lett. 42 (1983) 968.

[3] C. F. Guo, T. Sun, F. Cao, Q. Liu, Z. Ren, Light: Science & Applications 3 (2014) e161.

[4] A. Luque, A.V. Mellor, *Photon Absorption Models in Nanostructured Semiconductor Solar Cells and Devices*, SpringerBriefs in Applied Sciences and Technology, 2015. (DOI:10.1007/978-3-319-14538-9_1)

[5] *Photon Management in Solar Cells*, First Edition, Edited by R. B. Wehrspohn, U. Rau, A. Gombert, Wiley-VCH Verlab GmbH & Co. KGaA, 2015.

[6] F. J. Haug, C. Ballif, Energy Environ. Sci. 8 (2015) 824.

[7] M. L. Brongersma, Y. Cui, S. Fan, Nature Mater. 13 (2014) 451.

[8] H.-P. Wang, D. -H. Lien, M. -L. Tsai, C. -A. Lin, H. -C. Chang, K.-Y. Lai, Jr -H. He, J. Mater. Chem. C 2 (2014) 3144.

[9] J. -B. Orhan, R. Monnard, E. Vallat-Sauvain, L. Fesquet, D. Romang, X. Multone, J. -F. Boucher, J. Steinhauser, D. Dominé, J. -P. Cardoso, D. Borrello, G. Charitat, B. Dehbozorgi, G. Choong, M. Charrière, S. Benagli, J. Meier, J. Bailat, J. Escarré, N. Blondiaux, J. Sakurai, J. Lin, A. Matsunaga, P. Losio, Sol. Energ. Mat. Sol. Cells 140 (2015) 344-350.

[10] J. Zhu, Z. Yu, S. Fan, Y. Cui, Materials Science and Engineering R 70 (2010) 330.

[11] H. Xiao, J. Wang, H. Huang, L. Lu, Q. Lin, Z. Fan, X. Chen, C. Jeong, X. Zhu, D. Li, Nano Energy 11 (2015) 78-87.

[12] P. -Y. Chen, H. -H. Hsiao, C. -I. Ho, C. -C. Ho, W.-L. Lee, H. -C. Chang, S. -C. Lee, J. -Z. Chen, I. -C. Cheng, Opt. Express 22 (2014) A1128-A1136.

[13] S. Thiyagu, Z. Pei, M. –S. Jhong, Nanoscale Research Letters 7 (2012) 172.

[14] S. K. Ram, R. Rizzoli, D. Desta, B. R. Jeppesen, M. Bellettato, I. Samatov, Y. -C. Tsao, S. R. Johannsen, P. T. Neuvonen, T. G. Pedersen, R. N. Pereira, K. Pedersen, P. Balling, A. N. Larsen, J. Phys. D: Appl. Phys. 48 (2015) 365101.

[15] C. -M. Hsu, C. Battaglia, C. Pahud, Z. Ruan, F. -J. Haug, S. Fan, C. Ballif, Y. Cui, Adv. Energy Mater. 2 (2012) 628.

[16] H. Sai, K. Saito, N. Hozuki, M. Kondo, Appl. Phys. Lett. 102 (2013) 053509.

[17] D. Desta, S. K. Ram, R. Rizzoli, M. Bellettato, C. Summonte, B. R. Jeppesen, P. B. Jensen, Y.-C. Tsao, H. Wiggers, R. N. Pereira, P. Balling, A. N. Larsen, Nanoscale 8 (2016) 12035.

[18] S. Lin, E. K. Lee, N. Nguyen, M. Khine, Lab Chip 14 (2014) 3475.

[19] P. Rofouie, D. Pasini, A. D. Rey, J. Chem. Phys. 143 (2015) 114701.

[20] Q. Wang, X. Zhao, MRS Bulletin 41 (2016) 115.

[21] Y. Liu, J. Genzer, M. D. Dickey, Progress in Polymer Science 52 (2016) 79–106.

[22] A. Klukowska, M. Vogler, A. Kolander, F. Reuther, G. Gruetzner, M. Muehlberger, I. Bergmair, R. Schoeftner, Alternative Approach to Transparent Stamps for UV-based Nanoimprint Lithography – Techniques and Materials, *24th European Mask and Lithography Conference, Edited by Uwe F. W. Behringer, Proc. of SPIE* 6792 (2008) 67920J, [DOI: 10.1117/12.798602].

[23] I. G. Samatov, B. R. Jeppesen, A. N. Larsen, S. K. Ram, Appl. Phys. A 122 (2016) 458.

[24] M. Vetter, J. Andreu, J. P. Borrajo, A. Martin, J. A. Rodriguez, O. Agustsson, J. Schotsaert, K. Bittkau, R. Carius, A. Gordijn, A. Hoffmann, I. M. Macedo, J. K. Rath, R.E.I. Schropp,

A. Antony, J. Bertomeu, F. Kail, Development of High Performance Industrial TCO Glass for Very Large Area a-Si:H PV Modules. *Proc. 26th Europ. Photovoltaic Solar Energy Conf. & Exh., Hamburg, Germany*. **2011**, 2676 – 2679. (DOI:10.4229/26thEUPVSEC2011-3AV.2.28)

[25] COMSOL Multiphysics® v. 5.2. www.comsol.com. COMSOL AB, Stockholm, Sweden.

[26] W. Lee, S. –Y. Lee, J. Kim, S. C. Kim, B. Lee, Opt. Express 20 (2012) A941.

[27] M. Sarrazin, A. Herman, O. Deparis, Opt. Express 21 (2013) A616.

[28] A. D. Rakić, A. B. Djurišic, J. M. Elazar, M. L. Majewski, Appl. Opt. 37 (1998) 5271.

[29] J.-Y. Sun, S. Xia, M. -W. Moon, K. H. Oh, K. -S. Kim, Proc. R. Soc. A 468 (2012) 932.

[30] R. Dewan, S. Fischer, V.B. Meyer-Rochow, Y. Özdemir, S. Hamraz, D. Knipp, Bioinspiration & Biomimetics 7 (2011) 016003.

[31] A. V. Shah, H. Schade, M. Vanecek, J. Meier, E. Vallat-Sauvain, N. Wyrsch, U. Kroll, C. Droz, J. Bailat, Prog. Photovolt: Res. Appl. 12 (2004) 113.

[32] A. Tamang, A. Hongsingthong, V. Jovanov, P. Sichanugrist, B. A. Khan, R. Dewan, M. Konagai, D. Knipp, Sci. Rep. 6 (2016) 29639.

[33] K. J. Lee, J. Jin, B. –S. Bae, R. Magnusson, Guided-Mode Resonance Filters Fabricated with Soft Lithography*, Recent Advances in Nanofabrication Techniques and Applications*; Edited by B. Cui, InTech, **2011**. DOI: 10.5772/24028.

[34] T. Matsui, K. Maejima, A.Bidiville, H. Sai, T. Koida, T. Suezaki, M. Matsumoto, K. Saito, I. Yoshida, M. Kondo, J. J. Appl. Phys. 54 (2015) 08KB10.

[35] A. Lambertz, F. Finger, R. E. I. Schropp, U. Rau, V. Smirnov, Prog. Photovolt: Res. Appl. 23 (2015) 939–948.

Biosketch

Sanjay K. Ram is currently an associate professor in the Department of Physics and Astronomy at the Aarhus University in Denmark. He received his Ph.D. degree in physics from I.I.T. Kanpur, India in 2006. After postdoctoral fellowships at Ecole Polytechnique, France and FCT-UNL, Portugal, he joined Aarhus University in 2011. His research interests include semiconductor and metal oxide thin films; interface engineering for high performance silicon thin film solar cells; and low cost light management strategies for solar cells based on upconversion, plasmonics and photonics.

Derese Gugsa Desta received his M.Sc. in solid state physics from Addis Ababa University, Ethiopia in 2007; M.Sc. in nanoscience from University of Rovira I Virgili, Spain in 2008, and M.Sc. in material science from Aveiro University, Portugal in 2010. He worked as a lecturer at Dilla University, Ethiopia from 2011 to 2012, and as a research assistant at University of Aveiro from 2013 to 2015. He is currently pursuing Ph.D. in physics at the Institute for Materials Science, Hasselt University, Belgium. His research interests include thin film synthesis and characterization, nano-optics, and nanomaterials.

Rita Rizzoli received her doctoral degree in physics 'summa cum laude' from Bologna University, Italy in 1983. Since 1988, she is a researcher at the CNR - IMM Institute in Bologna, where she is responsible for the research line “Synthesis and characterization of C and Si based nanostructured materials for applications in sensors and nanoelectronics”. Her research interests include study of amorphous/c-Si heterojunction solar cells; PECVD deposition of thin film silicon and periodic amorphous multilayers based on Si alloys; catalytic-CVD deposition of carbon nanotubes and graphene for applications such as field-emission electron micro-sources, NEMS/MEMS thermoelectric devices, photovoltaic and optoelectronic devices.

Bruno Falcão received his B.Sc. (2009) and M.Sc. (2011) degrees in physics engineering from University of Aveiro (UA), Portugal, where he is currently pursuing the Ph.D. degree. He is a member of Institute for Nanostructures, Nanomodelling and Nanofabrication (i3N), Portugal, since 2010, and has worked as a teaching assistant between 2012 and 2015 at UA. His research interests focuses on the research of the structural, optical and electrical properties of low-dimensional semiconductors for photovoltaic applications, and on the investigation of silicon-based solar cells.

Emil Haldrup Eriksen received his bachelor's and master's degree in physics from the Department of Physics and Astronomy at the University of Aarhus, Denmark. He is currently pursuing his Ph.D. in physics at the University of Aarhus. His research interests include the modeling of complex physical phenomena, in particular within the context of renewable energy.

Michele Bellettato obtained his bachelor's degree in physics from the Alma Mater Studiorum of Bologna in 2009. Since 2010 he is working at CNR - IMM Institute in Bologna as vacuum, PECVD and Ion Implantation technician.

Bjarke Rolighed Jeppesen is a cleanroom process manager at the Interdisciplinary Nanoscience Center, Aarhus University. He received his master´s degree in physics from the Department of Physics and Astronomy, Aarhus University in 2013. His research interests focus on the synthesis of nanomaterials, plasmonic nanostructures, and photovoltaics.

Pia Bomholt Jensen is a laboratory technician at Department of Physics and Astronomy, and iNano Aarhus University. She joined the Department of Physics and Astronomy, Aarhus University in 1993 and the clean room facility at the Interdisciplinary Nanoscience Center, Aarhus University in 2009. Her research interests lie in semiconductor material synthesis, nanofabrication and characterization techniques.

Caterina Summonte received her doctoral degree in physics from the University of Bologna, Italy in 1982. She is a full-time researcher at CNR - IMM Institute in Bologna, Italy since 1988. She is active in the field of silicon-based photovoltaics; physics and technology of micro/nanocrystalline and amorphous silicon and related alloys, silicon nanodots, and optical characterization of materials. She deals with plasma deposition of nanocrystalline and epitaxial silicon deposited at low temperature, chemical transport deposition, and VHF plasma growth.

Rui N. Pereira received his Ph.D. in Physics in 2002 from University of Aveiro (UA), Portugal. He then moved to University of Aarhus, Denmark, to investigate defects in bulk and nanocrystal semiconductors. He was a postdoctoral researcher at Walter Schottky Institute (WSI), Technical University Munich, from 2006 to 2008 and afterward took a Researcher position at I3N, UA. In 2013 he was awarded a FCT Principal Researcher Grant at I3N and was appointed Research Staff at WSI. His present research is on electronic, optical, and magnetic properties of semiconductor nanocrystals for (opto)electronics and electronic surface properties of III-nitrides for photocatalysis.

Arne Nylandsted Larsen received his Ph.D. degree in physics in 1978 and his Dr.Scient. degree in physics in 1996, both from Aarhus University, Denmark. His research has focused on defects and impurity diffusion in semiconductors, and on the interaction of light with nanostructures. He is now professor emeritus.

Peter Balling obtained his Ph.D. in physics from the University of Aarhus, Denmark in 1995. He then worked as a post-doc at the Lawrence Berkeley National Lab, CA (Shank group). He is now back at the University of Aarhus, Denmark, where he as a professor is leading a research group covering several activities in light – matter interactions: ultrashort-pulse laser excitation of materials (experiments and modeling), semiconductor physics (e.g. applications in photovoltaics), and medical physics (optically based 3D radiation dosimetry).

Graphical Abstract

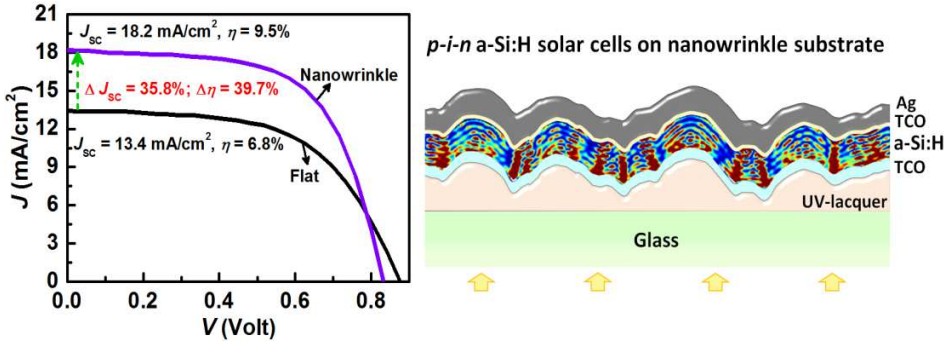

Article type: (Full Paper)

Title: Efficient light-trapping with quasi-periodic uniaxial nanowrinkles for thin-film silicon solar cells

Sanjay K. Ram[a,*], Derese Desta[b], Rita Rizzoli[c], Bruno P. Falcão[b], Emil H. Eriksen[a], Michele Bellettato[c], Bjarke R. Jeppesen[a], Pia B. Jensen[a], Caterina Summonte[c], Rui N. Pereira[b,d], Arne Nylandsted Larsen[a], Peter Balling[a]

[a]Department of Physics and Astronomy – iNANO, Aarhus University, Gustav Wieds Vej 14, DK-8000 Aarhus C, Denmark

[b]Department of Physics and I3N, University of Aveiro, Campus Universitário de Santiago, 3810-193 Aveiro, Portugal

[c]Istituto per la Microelettronica e Microsistemi (IMM)-Consiglio Nazionale delle Ricerche, via Gobetti 101, 40129, Bologna, Italy

[d]Walter Schottky Institut and Physik-Department, Technische Universität München, Am Coulombwall 4, 85748 Garching, Germany

*Address correspondence to E-mail: sanjayk.ram@inano.au.dk; sanjayk.ram@gmail.com